Earth's Energy Imbalance: Confirmation and Implications

James Hansen,[1,2]* Larissa Nazarenko,[1,2] Reto Ruedy,[3] Makiko Sato,[1,2] Josh Willis,[4] Anthony Del Genio,[1,5] Dorothy Koch,[1,2] Andrew Lacis,[1,5] Ken Lo,[3] Surabi Menon,[6] Tica Novakov,[6] Judith Perlwitz,[1,2] Gary Russell,[1] Gavin A. Schmidt,[1,2] Nicholas Tausnev[3]

Our climate model, driven mainly by increasing human-made greenhouse gases and aerosols, among other forcings, calculates that Earth is now absorbing 0.85 ± 0.15 watts per square meter more energy from the Sun than it is emitting to space. This imbalance is confirmed by precise measurements of increasing ocean heat content over the past 10 years. Implications include (i) the expectation of additional global warming of about 0.6°C without further change of atmospheric composition; (ii) the confirmation of the climate system's lag in responding to forcings, implying the need for anticipatory actions to avoid any specified level of climate change; and (iii) the likelihood of acceleration of ice sheet disintegration and sea level rise.

Earth's climate system has considerable thermal inertia. This point is of critical importance to policy- and decision-makers who seek to mitigate the effects of undesirable anthropogenic climate change. The effect of the inertia is to delay Earth's response to climate forcings, i.e., changes of the planet's energy balance that tend to alter global temperature. This delay provides an opportunity to reduce the magnitude of anthropogenic climate change before it is fully realized, if appropriate action is taken. On the other hand, if we wait for more overwhelming empirical evidence of climate change, the inertia implies that still greater climate change will be in store, which may be difficult or impossible to avoid.

The primary symptom of Earth's thermal inertia, in the presence of an increasing climate forcing, is an imbalance between the energy absorbed and emitted by the planet. This imbalance provides an invaluable measure of the net climate forcing acting on Earth. Improved ocean temperature measurements in the past decade, along with high-precision satellite altimetry measurements of the ocean surface, permit an indirect but precise quantification of Earth's energy imbalance. We compare observed ocean heat storage with simulations of global climate change driven by estimated climate forcings, thus obtaining a check on the climate model's ability to simulate the planetary energy imbalance.

The lag in the climate response to a forcing is a sensitive function of equilibrium climate sensitivity, varying approximately as the square of the sensitivity (*1*), and it depends on the rate of heat exchange between the ocean's surface mixed layer and the deeper ocean (*2*–*4*). The lag could be as short as a decade, if climate sensitivity is as small as 0.25°C per W/m^2 of forcing, but it is a century or longer if climate sensitivity is 1°C per W/m^2 or larger (*1*, *3*). Evidence from Earth's history (*3*–*6*) and climate models (*7*) suggests that climate sensitivity is 0.75° ± 0.25°C per W/m^2, implying that 25 to 50 years are needed for Earth's surface temperature to reach 60% of its equilibrium response (*1*).

We investigate Earth's energy balance via computations with the current global climate model of the NASA Goddard Institute for Space Studies (GISS). The model and its simulated climatology have been documented (*8*), as has its response to a wide variety of climate forcing mechanisms (*9*). The climate model's equilibrium sensitivity to doubled CO_2 is 2.7°C (~2/3°C per W/m^2) (*10*).

Climate forcings. Figure 1A summarizes the forcings that drive the simulated 1880 to 2003 climate change. Among alternative definitions of climate forcing (*9*), we use the effective forcing, F_e. F_e differs from conventional climate forcing definitions (*11*) by accounting for the fact that some forcing mechanisms have a lesser or greater "efficacy" in altering global temperature than an equal forcing by CO_2 (*9*). F_e is an energy flux change arising in response to an imposed forcing agent. It is constant throughout the atmosphere, because it is evaluated after atmospheric temperature has been allowed to adjust to the presence of the forcing agent.

The largest forcing is due to well-mixed greenhouse gases (GHGs)—CO_2, CH_4, N_2O, CFCs (chlorofluorocarbons)—and other trace gases, totaling 2.75 W/m^2 in 2003 relative to the 1880 value (Table 1). Ozone (O_3) and stratospheric H_2O from oxidation of increasing CH_4 bring the total GHG forcing to 3.05 W/m^2 (*9*). Estimated uncertainty in the total GHG forcing is ~15% (*11*, *12*).

Atmospheric aerosols cause climate forcings by reflecting and absorbing radiation, as well as through indirect effects on cloud cover and cloud albedo (*11*). The aerosol scenario in our model uses estimated anthropogenic emissions from fuel use statistics and includes temporal changes in fossil-fuel use technologies (*13*). Our parameterization of aerosol indirect effects (*9*, *14*) is constrained by empirical evidence that the aerosol indirect forcing is ~ −1 W/m^2 (*9*). The effective aerosol forcing in 2003 relative to that in 1880, including positive forcing by absorbing black carbon aerosols, is –1.39 W/m^2, with a subjective estimated uncertainty of ~50%.

Stratospheric aerosols from volcanoes cause a sporadically large negative forcing, with an uncertainty that increases with age from 15% for the 1991 Mount Pinatubo eruption to 50% for the 1883 Krakatau eruption (*9*). Land use and snow albedo forcings are small on a global average and uncertain by about a factor of 2 (*9*). Solar irradiance is taken as increasing by 0.22 W/m^2 between 1880 and 2003, with an estimated uncertainty of a factor of 2 (*9*). All of these partly subjective uncertainties are intended as 2σ error bars. The net change of effective forcing between 1880 and 2003 is +1.8 W/m^2, with a formal uncertainty of ±0.85 W/m^2 due almost entirely to aerosols (Table 1).

Climate simulations. The global mean temperature simulated by the GISS model driven by this forcing agrees well with observations (Fig. 1B). An ensemble of five simulations was obtained by using initial conditions at intervals of 25 years of the climate model control run, thus revealing the model's inherent unforced variability. The spatial distribution of the simulated warming (fig. S1) is slightly excessive in the tropics, as much as a few tenths of a degree Celsius, and on average the simulated warming is a few tenths of a degree Celsius less than that observed in middle latitudes of the Northern Hemisphere, but there is substantial variation from one model run to another (fig. S1).

[1]NASA Goddard Institute for Space Studies, New York, NY 10025, USA. [2]Columbia Earth Institute, Columbia University, New York, NY 10025, USA. [3]SGT Incorporated, New York, NY 10025, USA. [4]Jet Propulsion Laboratory, Pasadena, CA 91109, USA. [5]Department of Earth and Environmental Sciences, Columbia University, New York, NY 10025, USA. [6]Lawrence Berkeley National Laboratory, Berkeley, CA 94720, USA.

*To whom correspondence should be addressed. E-mail: jhansen@giss.nasa.gov

Discrepancy in the spatial distribution of warming may be partly a result of the uncertain aerosol distribution, specifically the division of aerosols between fossil-fuel and biomass-burning aerosols (*9*). However, excessive tropical warming in our model is primarily in the Pacific Ocean, where our coarse-resolution ocean model is unable to simulate climate variations associated with El Niño–Southern Oscillation processes.

The planetary energy imbalance in our model (Fig. 1C) did not exceed a few tenths of 1 W/m^2 before the 1960s. Since then, except for a few years following each large volcanic eruption, the simulated planetary energy imbalance has grown steadily. According to the model, Earth is now absorbing 0.85 ± 0.15 W/m^2 more solar energy than it radiates to space as heat.

Ocean heat storage. Confirmation of the planetary energy imbalance can be obtained by measuring the heat content of the ocean, which must be the principal reservoir for excess energy (*3*, *15*). Levitus *et al*. (*15*) compiled ocean temperature data that yielded increased ocean heat content of about 10 W year/m^2, averaged over the Earth's surface, during 1955 to 1998 [1 W year/m^2 over the full Earth ~ 1.61 × 10^{22} J; see table S1 for conversion factors of land, air, water, and ice temperature changes and melting to global energy units]. Total ocean heat storage in that period is consistent with climate model simulations (*16*–*19*), but the models do not reproduce reported decadal fluctuations. The fluctuations may be a result of variability of ocean dynamics (*17*) or, at least in part, an artifact of incomplete sampling of a dynamically variable ocean (*18*, *19*).

Improved definition of Earth's energy balance is possible for the past decade. First, the predicted energy imbalance due to increasing GHGs has grown to 0.85 ± 0.15 W/m^2, and the past decade has been uninterrupted by any large volcanic eruption (Fig. 1). Second, more complete ocean temperature data are available, including more profiling floats and precise satellite altimetry that permits improved estimates in data-sparse regions (*20*).

Figure 2 shows that the modeled increase of heat content in the past decade in the upper 750 m of the ocean is 6.0 ± 0.6 (mean ± SD) W year/m^2, averaged over the surface of Earth, varying from 5.0 to 6.6 W year/m^2 among five simulations. The observed annual mean rate of ocean heat gain between 1993 and mid-2003 was 0.86 ± 0.12 W/m^2 per year for the 93.4% of the ocean that was analyzed (*20*). Assuming the same rate for the remaining 6.6% of the ocean yields a global mean heat storage rate of 0.7 × 0.86 = 0.60 ± 0.10 W/m^2 per year or 6 ± 1 W year/m^2 for 10 years, 0.7 being the ocean fraction of Earth's surface. This agrees well with the 5.5 W year/m^2 in the analysis of Levitus *et al*. (*21*) for the upper 700 m that was based only on in situ data.

Figure 3 compares the latitude-depth profile of the observed ocean heat content change with the five climate model runs and the mean of the five runs. There is a large variability among the model runs, revealing the chaotic ''ocean weather'' fluctuations that occur on such a time scale. This variability is even more apparent in maps of change in ocean heat content (fig. S2). Yet the model runs contain essential features of observations, with deep penetration of heat anomalies at middle to high latitudes and shallower anomalies in the tropics.

The modeled heat gain of ~0.6 W/m^2 per year for the upper 750 m of the ocean differs from the decadal mean planetary energy imbalance of ~0.75 W/m^2 primarily because of heat storage at greater depths in the ocean. On average for the five simulations, 85% of the ocean heat storage occurred above 750 m, with the range from 78 to 91%. The mean heat gain below 750 m was ~0.11 W/m^2. The remaining 0.04 W/m^2 warmed the atmosphere and land and melted sea ice and land ice (see supplementary information).

Earth's energy imbalance. We infer from the consistency of observed and modeled planetary energy gains that the forcing still driving climate change, i.e., the forcing not yet responded to, averaged ~0.75 W/m^2 in the past decade and was ~0.85 ± 0.15 W/m^2 in 2003 (Fig. 1C). This imbalance is consistent with the total forcing of ~1.8 W/m^2 relative to that in 1880 and climate sensitivity of ~2/3°C per W/m^2. The observed 1880 to 2003 global warming is 0.6° to 0.7°C (*11*, *22*), which is the full response to nearly 1 W/m^2 of forcing. Of the 1.8 W/m^2 forcing, 0.85 W/m^2 remains, i.e., additional global warming of 0.85 × 0.67 ~ 0.6°C is ''in the pipeline'' and will occur in the future even if atmospheric composition and other

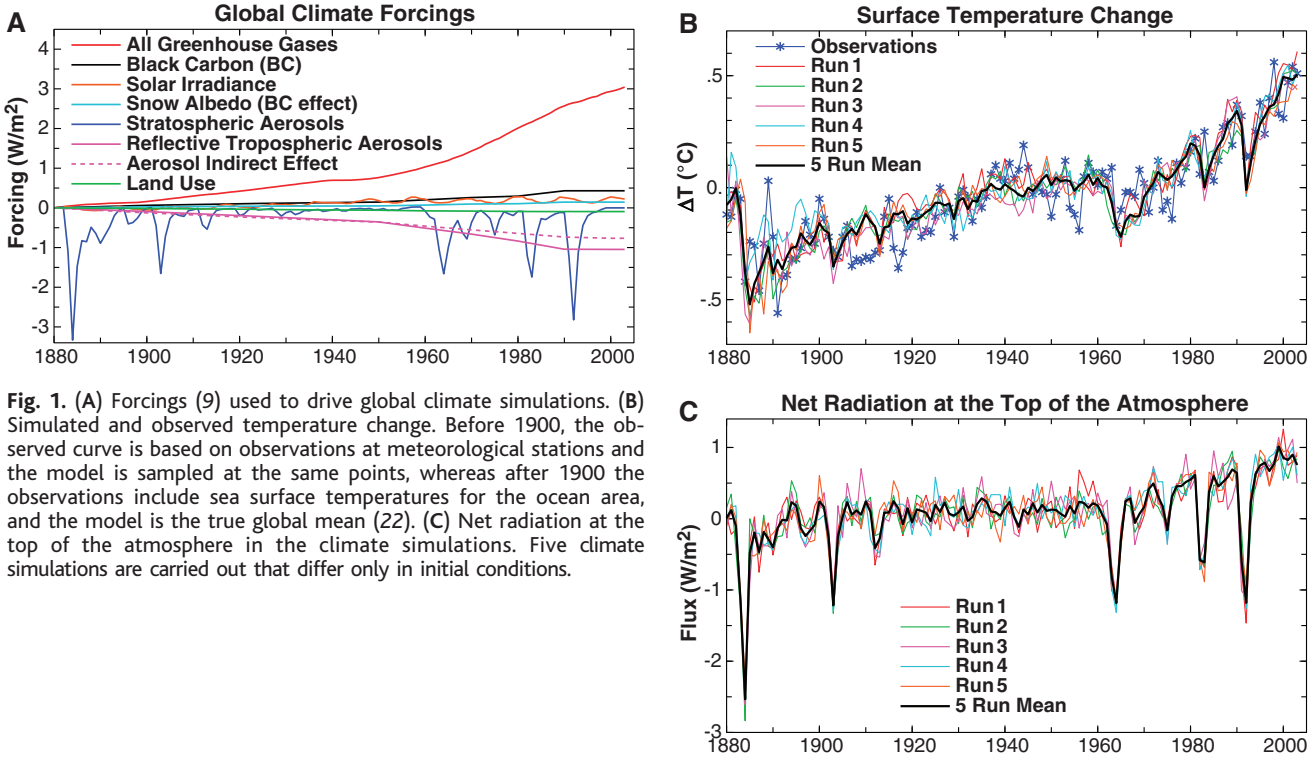

Fig. 1. (**A**) Forcings (*9*) used to drive global climate simulations. (**B**) Simulated and observed temperature change. Before 1900, the observed curve is based on observations at meteorological stations and the model is sampled at the same points, whereas after 1900 the observations include sea surface temperatures for the ocean area, and the model is the true global mean (*22*). (**C**) Net radiation at the top of the atmosphere in the climate simulations. Five climate simulations are carried out that differ only in initial conditions.

climate forcings remain fixed at today's values (*3*, *4*, *23*).

The present planetary energy imbalance is large by standards of Earth's history. For example, an imbalance of 1 W/m^2 maintained for the last 10,000 years of the Holocene is sufficient to melt ice equivalent to 1 km of sea level (if there were that much ice) or raise the temperature of the ocean above the thermocline by more than 100°C (table S1). Clearly, on long time scales, the planet has been in energy balance to within a small fraction of 1 W/m^2.

An alternative interpretation of the observed present high rate of ocean heat storage might be that it results, not from climate forcings, but from unforced atmosphere-ocean fluctuations. However, if a fluctuation had brought cool water to the ocean surface, as needed to decrease outgoing heat flux, the ocean surface would have cooled, whereas in fact it warmed (*22*). A positive climate forcing, anticipated independently, is the more viable interpretation.

The present 0.85 W/m^2 planetary energy imbalance, its consistency with estimated growth of climate forcings over the past century (Fig. 1A), and its consistency with the temporal development of global warming based on a realistic climate sensitivity for doubled CO_2 (Fig. 1B) offer strong support for the inference that the planet is out of energy balance because of positive climate forcings. If climate sensitivity, climate forcings, and ocean mixing are taken as arbitrary parameters (*24*), one may find other combinations that yield warming comparable to that of the past century. However, (i) climate sensitivity is constrained by empirical data; (ii) our simulated depth of penetration of ocean-warming anomalies is consistent with observations (fig. S2), thus supporting the modeled rate of ocean mixing; and (iii) despite ignorance about aerosol changes, there is sufficient knowledge to constrain estimates of climate forcings (*9*).

The planetary energy imbalance and implied warming "in the pipeline" complicate the task of avoiding any specified level of global warming. For example, it has been argued, on the basis of sea level during previous warm periods, that global warming of more than 1°C above the level of 2000 would constitute "dangerous anthropogenic interference" with climate (*25*, *26*). With 0.6°C global warming "in the pipeline" and moderate growth of non-CO_2 forcings, a 1°C limit on further warming limits peak CO_2 to about 440 parts per million (ppm) (*12*). Given the current CO_2 concentration of ~378 ppm, annual growth of ~1.9 ppm (*12*), and a still expanding worldwide fossil-fuel energy infrastructure, it may be impractical to avoid a CO_2 concentration of 440 ppm. A conceivable, though difficult, reduction of non-CO_2 forcings could increase the peak CO_2 limit for 1°C warming to a more feasible 520 ppm (*12*). This example illustrates that the 0.6°C unrealized warming associated with the planet's energy imbalance implies the need for near-term anticipatory actions, if a low limit on climate change is to be achieved.

Sea level. Sea level change includes steric (mainly thermal expansion) and eustatic (mainly changes of continental ice and other continental water storage) components. Observed temperature changes in the upper 700 to 750 m yield a steric sea level rise of 1.4 to 1.6 cm (*20*, *21*). The full ocean temperature changes in our five simulations yield a mean steric 10-year sea level increase of 1.6 cm. Our climate model does not include ice sheet dynamics, so we cannot calculate eustatic sea level change directly. Sea level measured by satellite altimeters since 1993 increased 2.8 ± 0.4 cm/decade (*27*), but as a measure of the volume change (steric + eustatic) of ocean water, this value must be increased by ~0.3 cm to account for the effect of global isostatic adjustment (*28*). We thus infer a eustatic contribution to sea level rise of ~1.5 cm in the past decade.

Both the rate of total sea level rise in the past decade and that of the eustatic component, which is a critical metric for ice melt, are accelerations over the rate of the preceding century. IPCC (*11*) estimated the rate of sea level rise of the past century to be 1.5 ± 0.5 cm/decade, with a central estimate of only 0.2 cm/decade for the eustatic component, albeit with a large uncertainty. Decadal var-

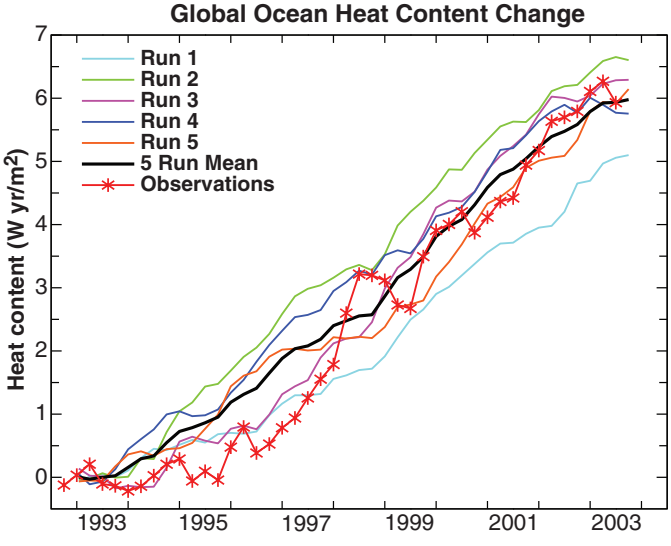

Fig. 2. Ocean heat content change between 1993 and 2003 in the top 750 m of world ocean. Observations are from (*20*). Five model runs are shown for the GISS coupled dynamical ocean-atmosphere model (*8*, *9*).

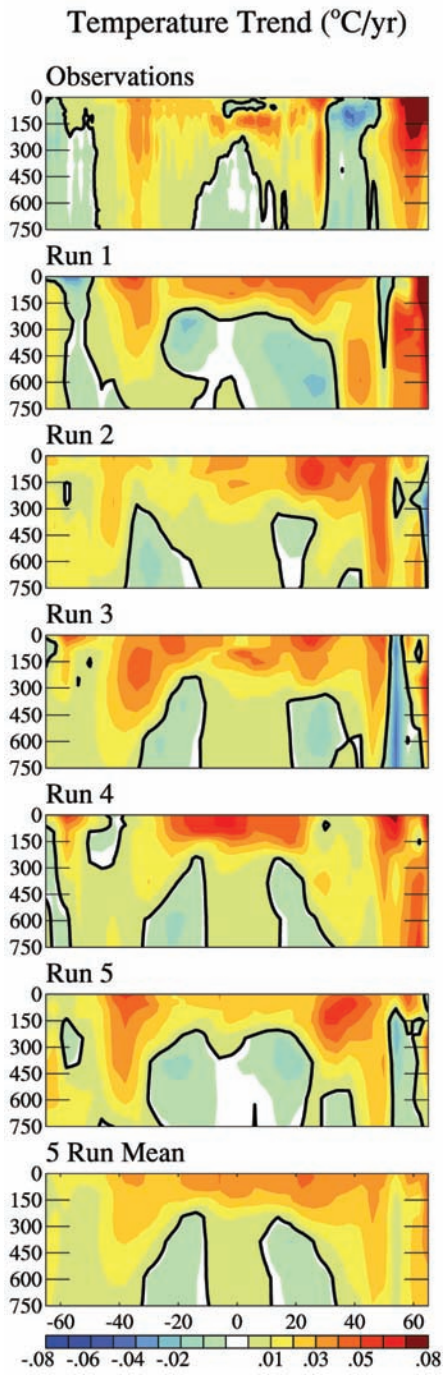

Fig. 3. Trend of zonally averaged temperature versus depth and latitude. Observations are from (*20*). The five model runs are as in Fig. 2.

iability limits the significance of sea level change in a single decade (*28*, *29*). However, we suggest that both the steric and eustatic increases are a product of the large, unusual, persistent planetary energy imbalance that overwhelms normal variability and as such may be a harbinger of accelerating sea level change (*26*).

The estimated ~1.5-cm eustatic sea level rise in the past decade, even if entirely due to ice melt, required only 2% of Earth's present energy imbalance (table S1). Much more rapid melt is possible if iceberg discharge is accelerating, as some recent observations suggest (*30*, *31*), and has occurred in past cases of sharp sea level rise that accompanied rapid global warming (*32*). Unlike ice sheet growth, which is limited by the snowfall rate in cold dry regions, ice sheet disintegration can be a wet process fed by multiple radiative and dynamical feedbacks (*26*). Thus, the portion of the planetary energy imbalance used for melting is likely to rise as the planet continues to warm, summer melt increases, and melt-water lubricates and softens the ice sheets. Other positive feedbacks include reduced ice sheet albedo, a lowering of the ice sheet surface, and effects of rising sea level on coastal ice shelves (*26*).

Table 1. Effective climate forcings (W/m^2) used to drive the 1880 to 2003 simulated climate change in the GISS climate model (*9*).

Forcing agent*		Forcing (W/m^2)
Greenhouse gases (GHGs)	–	–
Well-mixed GHGs	2.75	–
Ozone†‡	0.24	–
CH_4-derived stratospheric H_2O	0.06	–
Total: GHGs		3.05 ± 0.4
Solar irradiance		0.22 (×2)
Land use		−0.09 (×2)
Snow albedo		0.14 (×2)
Aerosols		
Volcanic aerosols	0.00	–
Black carbon‡	0.43	–
Reflective tropospheric aerosols	−1.05	–
Aerosol indirect effect	−0.77	–
Total: aerosols	–	−1.39 ± 0.7
Sum of individual forcings	–	1.93
All forcings at once	–	1.80 ± 0.85

*Effective forcings are derived from five-member ensembles of 120-year simulations for each individual forcing and for all forcings acting at once [see (*9*) and supporting online material]. The sum of individual forcings differs slightly from all forcings acting at once because of nonlinearities in combined forcings and unforced variability in climate simulations. †This is the ozone forcing in our principal IPCC simulations; it decreases from 0.24 to 0.22 W/m^2 when the stratospheric ozone change of Randel and Wu (S1) is used [see (*9*) and supporting online material]. ‡Ozone and black carbon forcings are less than they would be for conventional forcing definitions (*11*), because their "efficacy" is only ~75% (*9*).

Implications. The thermal inertia of the ocean, with resulting unrealized warming "in the pipeline," combines with ice sheet inertia and multiple positive feedbacks during ice sheet disintegration to create the possibility of a climate system in which large sea level change is practically impossible to avoid. If the ice sheet response time is millennia, the ocean thermal inertia and ice sheet dynamical inertia are relatively independent matters. However, based on the saw-toothed shape of glacial-interglacial global temperature and qualitative arguments about positive feedbacks, substantial ice sheet change could occur on the time scale of a century (*26*).

The destabilizing effect of comparable ocean and ice sheet response times is apparent. Assume that initial stages of ice sheet disintegration are detected. Before action to counter this trend could be effective, it would be necessary to eliminate the positive planetary energy imbalance, now ~0.85 W/m^2, which exists as a result of the ocean's thermal inertia. Given energy infrastructure inertia and trends in energy use, that task could require on the order of a century to complete. If the time for a substantial ice response is as short as a century, the positive ice-climate feedbacks imply the possibility of a system out of our control.

A caveat accompanying our analysis concerns the uncertainty in climate forcings. A good fit of observed and modeled temperatures (Fig. 1) also could be attained with smaller forcing and larger climate sensitivity, or with the converse. If climate sensitivity were higher (and forcings smaller), the rate of ocean heat storage and warming "in the pipeline" or "committed" would be greater, e.g., models with a sensitivity of 4.2° to 4.5°C for doubled CO_2 yield ~1°C "committed" global warming (*3*, *4*). Conversely, smaller sensitivity and larger forcing yield lesser committed warming and ocean heat storage. The agreement between modeled and observed heat storage (Fig. 2) favors an intermediate climate sensitivity, as in our model. This test provided by ocean heat storage will become more useful as the period with large energy imbalance continues.

Even if the net forcing is confirmed by continued measurement of ocean heat storage, there will remain much room for tradeoffs among different forcings. Aerosol direct and indirect forcings are the most uncertain. The net aerosol forcing that we estimate, −1.39 W/m^2, includes a large positive forcing by black carbon and a negative aerosol indirect forcing. Both of these aerosol forcings reduce sunlight reaching the surface and may be the prime cause of observed "global dimming" (*33*) and reduced pan evaporation (*34*).

Given the unusual magnitude of the current planetary energy imbalance and uncertainty about its implications, careful monitoring of key metrics is needed. Continuation of the ocean temperature and altimetry measurements is needed to confirm that the energy imbalance is not a fluctuation and to determine the net climate forcing acting on the planet. The latter is a measure of the changes that will be needed to stabilize climate. Understanding of the forcings that give rise to the imbalance requires more precise information on aerosols (*35*). The high rate of recent eustatic sea level rise that we infer suggests positive contributions from Greenland, alpine glaciers, and West Antarctica. Quantification of these sources is possible using precise satellite altimetry and gravity measurements as initiated by the IceSat (*36*) and GRACE satellites (*37*), which warrant follow-on missions.

References and Notes

1. J. Hansen *et al.*, *Science* **229**, 857 (1985).
2. M. I. Hoffert, A. J. Callegari, C. T. Hsieh, *J. Geophys. Res.* **85**, 6667 (1980).
3. J. Hansen *et al.*, *Am. Geophys. Union Geophys. Monogr. Ser.* **29**, 130 (1984).
4. T. M. L. Wigley, M. E. Schlesinger, *Nature* **315**, 649 (1985).
5. M. I. Hoffert, C. Covey, *Nature* **360**, 573 (1992).
6. J. Hansen, A. Lacis, R. Ruedy, M. Sato, H. Wilson, *Natl. Geogr. Res. Explor.* **9**, 143 (1993).
7. R. Kerr, *Science* **305**, 932 (2004).
8. G. A. Schmidt *et al.*, in preparation.
9. J. Hansen *et al.*, *J. Geophys. Res.*, in preparation.
10. The climate simulations for 1880 to 2003 used here will be included in the Intergovernmental Panel on Climate Change (IPCC) 2007 report and are available with other IPCC runs at http://www-pcmdi.llnl.gov/ipcc/about_ipcc.php or via www.giss.nasa.gov/data/imbalance.
11. Intergovernmental Panel on Climate Change (IPCC), *Climate Change 2001: The Scientific Basis*, J. T. Houghton *et al.*, Eds. (Cambridge Univ. Press, New York, 2001).
12. J. Hansen, M. Sato, *Proc. Natl. Acad. Sci. U.S.A.* **101**, 16,109 (2004).
13. T. Novakov *et al.*, *Geophys. Res. Lett.* **30**, 1324 (2003).
14. S. Menon, A. Del Genio, in preparation.
15. S. Levitus, J. I. Antonov, T. P. Boyer, C. Stephens, *Science* **287**, 2225 (2000).
16. S. Levitus *et al.*, *Science* **292**, 267 (2001).
17. T. P. Barnett, D. W. Pierce, R. Schnur, *Science* **292**, 270 (2001).
18. S. Sun, J. E. Hansen, *J. Clim.* **16**, 2807 (2003).
19. J. M. Gregory, H. T. Banks, P. A. Stott, J. A. Lowe, M. D. Palmer, *Geophys. Res. Lett.* **31**, L15312 (2004).
20. J. K. Willis, D. Roemmich, B. Cornuelle, *J. Geophys. Res.* **109**, C12036 (2004).
21. S. Levitus, J. I. Antonov, T. P. Boyer, *Geophys. Res. Lett.* **32**, L02604 (2004).
22. J. Hansen *et al.*, *J. Geophys. Res.* **106**, 23947 (2001).
23. R. T. Wetherald, R. J. Stouffer, K. W. Dixon, *Geophys. Res. Lett.* **28**, 1535 (2001).
24. R. S. Lindzen, *Geophys. Res. Lett.* **29**, 1254 (2002).
25. J. Hansen, *Sci. Am.* **290**, 68 (March 2004).
26. J. Hansen, *Clim. Change* **68**, 269 (2005).
27. E. W. Leuliette, R. S. Nerem, G. T. Mitchum, *Mar. Geodesy* **27**, 79 (2004).
28. B. C. Douglas, W. R. Peltier, *Phys. Today* **55**, 35 (2002).
29. W. Munk, *Proc. Natl. Acad. Sci. U.S.A.* **99**, 6550 (2002).
30. I. Joughin, W. Abdalati, M. Fahnestock, *Nature* **432**, 608 (2004).
31. R. Thomas *et al.*, *Science* **306**, 255 (2004).
32. G. Bond *et al.*, *Nature* **360**, 245 (1992).
33. B. Liepert, *Geophys. Res. Lett.* **29**, 1421 (2002).
34. M. L. Roderick, G. D. Farquhar, *Science* **298**, 1410 (2002).
35. M. I. Mishchenko *et al.*, *J. Quant. Spectrosc. Radiat. Transfer* **88**, 149 (2004).
36. H. J. Zwally *et al.*, *J. Geodyn.* **34**, 405 (2002).

37. B. D. Tapley, S. Bettadpur, J. C. Ries, P. F. Thompson, M. M. Watkins, *Science* **305**, 503 (2004).
38. We thank W. Abdalati, B. Chao, J. Dickey, W. Munk, and J. Zwally for helpful information; D. Cain for technical assistance; and J. Kaye, D. Anderson, P. DeCola, T. Lee, and E. Lindstrom (NASA Earth Science Research Division managers) and H. Harvey (Hewlett Foundation) for research support. These data were collected and made freely available by the International Argo Project and the national programs that contribute to it (www.argo.ucsd.edu, http://argo.jcommops.org). Argo is a pilot program of the Global Ocean Observing System.

Supporting Online Material
www.sciencemag.org/cgi/content/full/1110252/DC1
SOM Text
Figs. S1 and S2
Table S1
References

26 January 2005; accepted 19 April 2005
Published online 28 April 2005;
10.1126/science.1110252
Include this information when citing this paper.

Anchorless Prion Protein Results in Infectious Amyloid Disease Without Clinical Scrapie

Bruce Chesebro,[1]* Matthew Trifilo,[2] Richard Race,[1] Kimberly Meade-White,[1] Chao Teng,[2] Rachel LaCasse,[1] Lynne Raymond,[1] Cynthia Favara,[1] Gerald Baron,[1] Suzette Priola,[1] Byron Caughey,[1] Eliezer Masliah,[3] Michael Oldstone[2]

In prion and Alzheimer's diseases, the roles played by amyloid versus nonamyloid deposits in brain damage remain unresolved. In scrapie-infected transgenic mice expressing prion protein (PrP) lacking the glycosylphosphatidylinositol (GPI) membrane anchor, abnormal protease-resistant PrPres was deposited as amyloid plaques, rather than the usual nonamyloid form of PrPres. Although PrPres amyloid plaques induced brain damage reminiscent of Alzheimer's disease, clinical manifestations were minimal. In contrast, combined expression of anchorless and wild-type PrP produced accelerated clinical scrapie. Thus, the PrP GPI anchor may play a role in the pathogenesis of prion diseases.

Transmissible spongiform encephalopathies (TSEs) or prion diseases (*1*) include Creutzfeldt-Jakob disease (CJD) in humans, bovine spongiform encephalopathy or "mad cow dissease" in cattle, scrapie in sheep, and chronic wasting disease in deer and elk of North America. These diseases are similar to nontransmissible protein deposition diseases, such as the systemic amyloidoses and Alzheimer's disease, where a host-derived protein is misfolded and persists in an aggregated form that may damage nearby cells. Amyloid may be present in all these diseases; however, there are important differences among these disease families. In systemic amyloidoses, amyloid deposits in organs appear to be directly pathogenic (*2*), whereas in Alzheimer's disease, pre-amyloid forms (rather than amyloid itself) may be the major neuropathogenic moiety (*3*, *4*). In prion diseases, amyloid formation is variable and may contribute to pathogenesis (*5*). The host protein involved in misfolding and amyloid formation is PrP (*6*, *7*), and PrP is required for susceptibility to disease as well as replication of infectivity (*8*). After infection, normal protease-sensitive PrP (PrPsen) is converted to an aggregated partially protease-resistant structure (PrPres or PrP^{Sc}) (*9*) associated with brain pathology. Three basic patterns of PrPres deposition are found in prion diseases: diffuse "synaptic" nonamyloid deposits, coarse perivacuolar deposits, and dense plaque-like amyloid deposits (*10*, *11*). However, the relative roles of these PrPres forms in brain tissue damage are unknown.

In most cell types, the majority of PrPsen is expressed as a GPI-linked cell surface glycoprotein (*12*), but the role of this GPI membrane anchor in TSE disease is unclear. In cell-free experiments, PrP lacking the GPI moiety ("anchorless PrP") can be converted to the PrPres form (*13*, *14*). However, in scrapie-infected cells, absence of the GPI moiety reduces conversion (*15*, *16*), which suggests that conversion involves membrane-bound GPI-linked PrP. However, redirecting PrP to clathrin-coated pits on the plasma membrane by fusing PrP to a transmembrane domain blocks conversion to PrPres (*17*). Thus, GPI-negative (GPI^-) PrP might facilitate or inhibit susceptibility to TSE infection in vivo. Here, we tested the role of the PrP GPI anchor in scrapie infection and disease in transgenic mice expressing only GPI^- PrP.

Generation of GPI-negative PrP transgenic mice. The transgene was constructed by modifying the ''half-genomic'' mouse PrP plasmid pHGPrP (fig. S1) (*18*). Two transgenic (Tg) lines expressing the highest amounts of PrP (Tg23 and Tg44) were selected for experiments. In brains of Tg23 and Tg44 lines heterozygous for the transgene, PrP mRNA expression was half that in C57BL/6 control mice. Organ extracts were also analyzed for PrPsen expression. In brain, PrPsen levels were about one-fourth that in controls, and PrP was also noted in several other tissues (Fig. 1A). The protein was mainly in the unglycosylated form. In neurons isolated from Tg44 mice, PrP was not located on the cell surface, as is the case with GPI-linked PrP (Fig. 1B). However, levels of intracellular PrP in these mice were similar to controls, indicating that PrP did not accumulate abnormally in these cells. In floatation gradients using brain tissue, GPI^- PrP did not float with raft fractions, in contrast to wild-type GPI-linked PrP (fig. S2). In cell lines, GPI^- PrP was not detectable on the plasma membrane (fig. S3) but appeared in the endoplasmic reticulum and Golgi complex, and was secreted into the medium (*19*). Thus, GPI^- PrP differed markedly from wild-type PrP in subcellular localization and processing.

Infection with three scrapie strains. To study the susceptibility of GPI^- PrP Tg mice to scrapie infection, we inoculated Tg mice and non-Tg controls intracerebrally at 6 weeks of age with scrapie brain homogenate containing 0.7×10^6 to 1.0×10^6 ID_{50} (where ID_{50} is the dose causing disease in 50% of animals). Three scrapie strains [RML (Chandler), ME7, and 22L] (*20*, *21*) were tested to assess strain-dependent differences. Mice were observed daily for typical clinical signs of scrapie, including altered gait, kyphosis, ataxia, disorientation, somnolence, and wasting (Table 1). Clinical disease occurred within 140 to 160 days in control mice homozygous for endogenous wild-type mouse PrP, and within 240 to 260 days in heterozygous control mice. In contrast, in Tg23 and Tg44 mice, no clinical signs were observed after 600 days with the RML strain or 400 days with the ME7 strain. Two 22L-infected mice from line 23 developed a wasting syndrome without neurological signs and died at 370 days. Two other mice in this group showed no symptoms of disease after more than 550 days (Table 1), whereas 22L-infected mice from line 44 showed no symptoms after more than 440 days. Thus, the wasting syndrome in line Tg23 was unlikely related to scrapie infection. In summary, scrapie infection failed to induce the usual clinical manifestations of prion disease in these Tg mice.

Replication of scrapie agent. The lack of clinical disease raised the issue of whether

[1]Laboratory of Persistent Viral Diseases, Rocky Mountain Laboratories, National Institute of Allergy and Infectious Diseases, Hamilton, MT 59840, USA. [2]Division of Virology, Department of Neuropharmacology, Scripps Research Institute, La Jolla, CA 92037, USA. [3]Departments of Neurosciences and Pathology, University of California, San Diego, La Jolla, CA 92093, USA.

*To whom correspondence should be addressed. E-mail: bchesebro@niaid.nih.gov